

Enhanced Stability of Coated Carbon Electrode for Li-O₂ Batteries and Its Limitations

Youngjoon Bae, Dong-Hyun Ko, Sunyoung Lee, Hee-Dae Lim, Yun-Jung Kim, Hyun-Soo Shim, Hyeokjun Park, Youngmin Ko, Sung Kwan Park, Hyuk Jae Kwon, Hyunjin Kim, Hee-Tak Kim, Yo-Sep Min, Dongmin Im, and Kisuk Kang*

Li-O₂ batteries are promising next-generation energy storage systems because of their exceptionally high energy density ($\approx 3500 \text{ W h kg}^{-1}$). However, to achieve stable operation, grand challenges remain to be resolved, such as preventing electrolyte decomposition and degradation of carbon, a commonly used air electrode in Li-O₂ batteries. In this work, using in situ differential electrochemical mass spectrometry, it is demonstrated that the application of a ZnO coating on the carbon electrode can effectively suppress side reactions occurring in the Li-O₂ battery. By probing the CO₂ evolution during charging of ¹³C-labeled air electrodes, the major sources of parasitic reactions are precisely identified, which further reveals that the ZnO coating retards the degradation of both the carbon electrode and electrolyte. The successful suppression of the degradation results in a higher oxygen efficiency, leading to enhanced stability for more than 100 cycles. Nevertheless, the degradation of the carbon electrode is not completely prevented by the coating, because the Li₂O₂ discharge product gradually grows at the interface between the ZnO and carbon, which eventually results in detachment of the ZnO particles from the electrode and subsequent deterioration of the performance. This finding implies that surface protection of the carbon electrode is a viable option to enhance the stability of Li-O₂ batteries; however, fundamental studies on the growth mechanism of the discharge product on the carbon surface are required along with more effective coating strategies.

the lithium-oxygen (Li-O₂) chemistry offers one of the highest theoretical energy densities, which can reach 3500 W h kg^{-1} based on the reaction $2\text{Li}^+ + \text{O}_2 + 2\text{e}^- \rightarrow \text{Li}_2\text{O}_2$ ($E^0 = 2.96 \text{ V vs Li/Li}^+$).^[3,6,7] In a typical discharge reaction, oxygen is reduced and reacts with lithium ions to produce lithium peroxide (Li₂O₂), which is mainly deposited on the surface of the air electrode, and the reverse reaction occurs upon charging. The most widely used air electrodes are carbon-based materials because of their large surface areas per weight and high electrical conductivity, which are suitable for promoting the electrochemical formation of Li₂O₂ on the electrode, providing a high gravimetric energy density. For these reasons, carbon-based air electrodes have been intensely researched in recent years, and various types of carbon materials such as porous carbon, carbon nanotubes (CNTs), and graphene have been reported as air electrodes.^[8–18]


Recent studies, however, have shown that parasitic reactions involving carbon-based air electrodes could be one of the

1. Introduction

The increasing demands for electric vehicles have spurred a worldwide search for next-generation rechargeable batteries with higher energy density.^[1–5] Among various battery systems,

factors resulting in the deterioration of the electrochemical cycling of Li-O₂ batteries.^[19–22] Upon cycling, carbon can react with Li₂O₂, a discharge product deposited on the carbon electrode, to form insulating Li₂CO₃, which degrades the efficiency and cycle stability.^[19,20] Moreover, carbon itself can be corroded

Y. Bae, Dr. H.-D. Lim, H.-S. Shim, H. Park, Y. Ko, S. K. Park, Prof. K. Kang
Department of Materials Science and Engineering
Research Institute of Advanced Materials (RIAM)
Seoul National University
1 Gwanak-ro, Gwanak-gu, Seoul 151-742, Republic of Korea
E-mail: matlgen1@snu.ac.kr
D.-H. Ko, S. Lee, Y.-S. Min
Department of Chemical Engineering
Konkuk University
120 Neungdong-ro, Gwangjin-gu, Seoul 143-701, Republic of Korea

 The ORCID identification number(s) for the author(s) of this article can be found under <https://doi.org/10.1002/aenm.201702661>.

Y.-J. Kim, H.-T. Kim
Department of Chemical and Biomolecular Engineering
Korea Advanced Institute of Science and Technology
291 Daehak-ro, Yuseong-gu, Daejeon 305-701, Republic of Korea
Dr. H. J. Kwon, Dr. H. Kim, Dr. D. Im
Energy Material Lab
Material Research Center
Samsung Advanced Institute of Technology
Samsung Electronics Co., Ltd.
130 Samsung-ro, Yeongtong-gu, Suwon, Gyeonggi-do 16678, Republic of Korea

DOI: 10.1002/aenm.201702661

under high oxidizing potential in Li-O₂ batteries and can thus be passivated with carbon-containing byproducts.^[19,20] The damaged carbon surface aggravates the electrolyte decomposition, resulting in the formation of additional byproducts.^[22] These byproducts from the electrolyte and carbon electrode can be partially decomposed during charge and typically lead to the evolution of CO₂ gas instead of O₂. As the cycle continues, insulating byproducts are gradually accumulated, which generally results in a high overpotential, low round-trip efficiency, and short cycle life.^[23–25] Even though non-carbon-based air electrodes such as gold, silver, and TiC electrodes have been developed to overcome these issues, their costs and low specific capacities have limited their practical applications.^[26–28] Therefore, the design of a strategy to reduce side reactions in the carbon electrode is imperative to achieve high electrochemical stability of Li-O₂ batteries.^[29–31]

Our previous work demonstrated that defect sites on carbon materials are more susceptible to reaction with discharge products and are prone to decompose more easily, serving as seeds for side reactions.^[22] Thus, a carbon air electrode with higher crystallinity could exhibit more stable cycle properties. However, the preparation of highly crystalline carbon generally requires high-temperature treatment above 2000 °C and substantially reduces the surface area, leading to a relatively small discharge capacity.^[22] Moreover, the complete removal of the defects in the production of large-surface carbon materials is not trivial. Instead, appropriate passivation of defect sites for a given carbon material may be a suitable approach to fabricate stable carbon-based air electrodes. Selective growth of materials specifically on the defect sites with the minimal amount of coating would be ideal to prohibit the side reactions without excessively increasing the weight of the air electrode. It was previously reported that Al₂O₃ and Pd could be coated on carbon using atomic layer deposition (ALD) to protect the air electrode and reduce the overpotential, resulting in enhanced cycle stability.^[31] Nevertheless, the insulating nature of Al₂O₃ caused a large overpotential during cycling, and the high price of the noble metal remains an issue. Moreover, it is not clearly understood how and to what extent these coating materials can aid in the reduction of the side reactions and whether its effect is maintained with extended cycling.

Herein, we demonstrate that the effect of coating is not limited to the protection of the carbon electrode but also remarkably suppresses the decomposition of the electrolyte. These results were analyzed using in situ differential electrochemical mass spectrometry (DEMS) with labeled isotopic ¹³C air electrode in the electrolyte composed of ¹²C for the Li-O₂ cell. During electrochemical charge and discharge, byproducts from the electrolyte and carbon electrode were simultaneously detected to discern their origin by analyzing the ratio of ¹²CO₂ and ¹³CO₂ evolution. Moreover, the evolution of these ratios with cycling for coated electrodes was monitored, providing insight into the mechanism by which the coating enhances the cycling. Our findings demonstrate the importance of defect control on the carbon electrode and suggest that effective coating strategies are required for the optimal operation of carbon electrodes in Li-O₂ batteries along with providing further understanding of the growth mechanism of discharge products on the carbon surface.

2. Results and Discussion

In our study of the effects of coating, ZnO was coated on the carbon electrode using ALD.^[32–34] Although ALD method may not be practically feasible for the large-scale process, it was used to coat ZnO on the defect sites of carbon cathode homogeneously to model the cases to alter the state of defect sites in the controlled manner. In order to focus on the effect of coating on the stability of carbon air electrode, coating materials which have shown catalytic effects on the Li-O₂ chemistry such as Pt, Pd, Ru, RuO₂, and Co₃O₄ were ruled out.^[13,31,35–37] Since ZnO does not generally exhibit catalytic effect on the reactions of Li-O₂ battery and is relatively conductive, we chose ZnO as a model coating material. Based on the predetermined protocol for coating ZnO on carbon (see the Supporting Information), we prepared the ZnO-coated air electrode using isotope ¹³C. The use of isotope ¹³C enabled us to distinguish the relative stabilities of the carbon electrode and electrolyte based on the naturally abundant ¹²C, as will be discussed later. **Figure 1a,b** presents transmission electron microscopy (TEM) images of the pristine ¹³C and ZnO-coated ¹³C electrodes, respectively. The pristine electrode exhibited the microstructure of amorphous carbon, whereas ZnO was deposited on the surface of ¹³C in the form of nanoparticles for the ZnO-coated ¹³C electrode. **Figure 1c** presents the Zn 2p X-ray photoelectron spectroscopy (XPS) spectra of the electrodes with increasing number of ALD cycles of ZnO deposition (pristine ¹³C, 8-cyc ZnO/¹³C, and 15-cyc ZnO/¹³C). With increasing number of ALD cycles, the characteristic ZnO peaks at 1022.4 eV (Zn 2p_{3/2}) and 1045.4 eV (Zn 2p_{1/2}) became stronger, indicating more ZnO deposition on the carbon. Notably, the Raman analyses in **Figure 1d,e** reveal systematic changes in the I_D/I_G ratio with increasing ZnO thickness. On the magnified scale in **Figure 1e**, the I_D/I_G ratio decreased as more ZnO was deposited, indicating the reduction of the exposed defective (i.e., nongraphitic disordered) carbon in the structure.^[22,38] For the optimal deposition of ZnO on a conventional carbon electrode, a CNT electrode was used as a reference to precisely probe the amount and morphology of ZnO, and similar observations were made for the series of CNT-type electrodes with increasing number of ALD cycles of ZnO deposition, as described in the Supporting Information. This finding implies that the ZnO is preferably deposited on defect sites of the carbon surface and effectively shielded the defects in the structure.

To verify the effect of ZnO coating, two Li-O₂ cells were assembled using ¹³C air electrodes with and without the ZnO coating, as shown in **Figure 2**. The assembled Li-O₂ cells were composed of the respective carbon air electrodes, a protected Li metal anode, and tetraethylene glycol dimethylether (TEGDME) dissolved with 1 M lithium bis(trifluoromethane)sulfonimide (LiTFSI) and 0.05 M LiI as the electrolyte containing redox mediator.^[12,39–41] (The detailed cell configuration is provided in the Experimental Section.) **Figure 2a,b** displays the discharge–charge profiles and cycle stability of the Li-O₂ cell with the pristine ¹³C air electrode, respectively, compared with those of the ZnO-coated electrode (**Figure 2c,d**). The use of the redox mediator and protected Li metal aided in reducing the polarization and enhancing the cycle efficiency of the cell compared with conventional Li-O₂ cells.^[41]

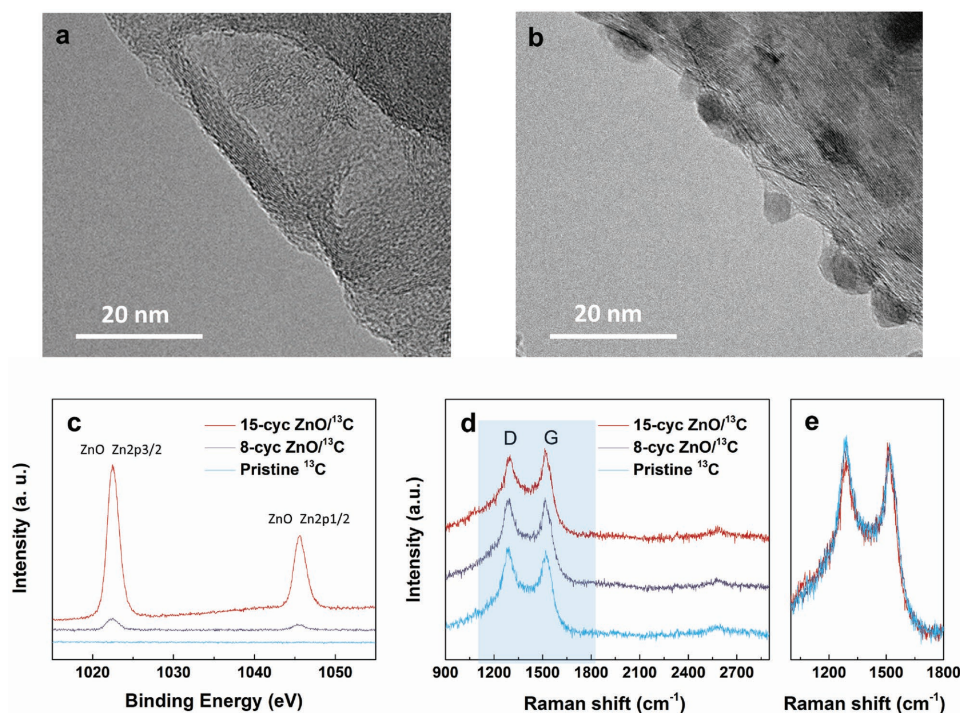


Figure 1. a) TEM image of pristine ^{13}C , b) TEM image of ZnO-coated ^{13}C , c) XPS spectra of pristine ^{13}C , 8-cyc ZnO/ ^{13}C , and 15-cyc ZnO/ ^{13}C , d) Raman spectra of pristine ^{13}C , 8-cyc ZnO/ ^{13}C , and 15-cyc ZnO/ ^{13}C , and e) magnified Raman spectra of (d).

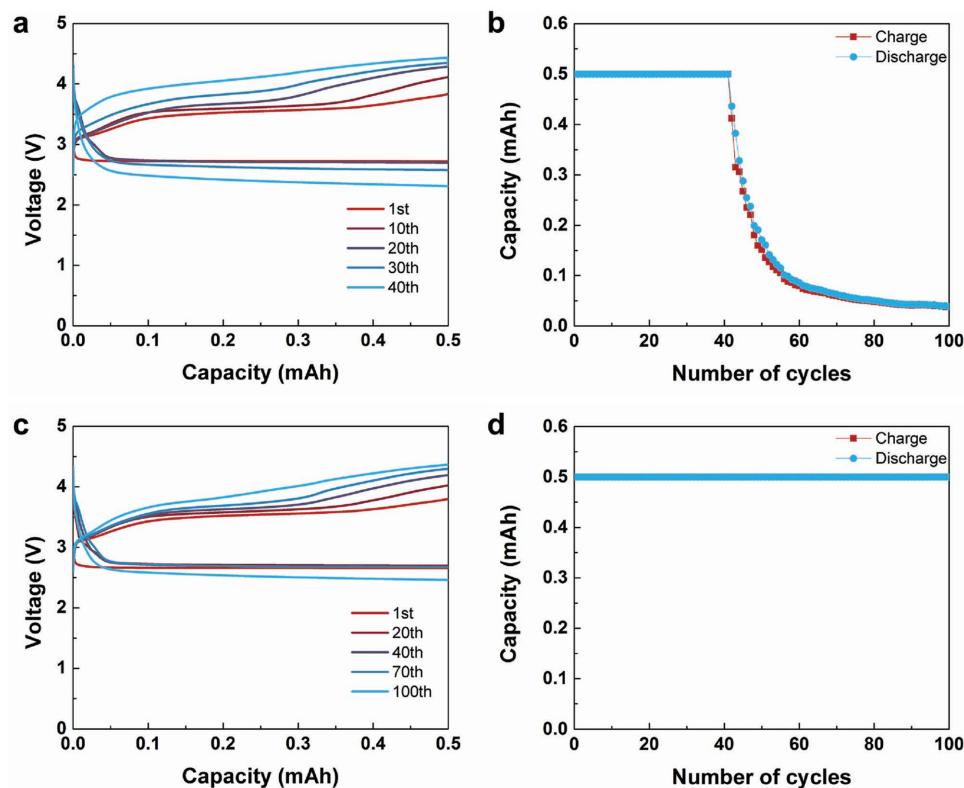


Figure 2. Discharge-charge profiles of Li-O₂ cells with the LiI redox mediator and CPL-protected Li metal using a) pristine ^{13}C and c) ZnO-coated ^{13}C as the air electrodes at a current rate of 0.1 mA cm^{-2} . Cycle stability of each Li-O₂ cell using the b) pristine ^{13}C and d) ZnO-coated ^{13}C as the air electrodes.

Nevertheless, it is noteworthy that the ZnO-coated air electrode further improved the cycle stability with relatively smaller overpotentials being maintained throughout the cycles. For the pristine electrode in Figure 2a,b, the charging overpotential gradually increased, leading to rapid cycle degradation after 40 cycles. The increase in the overpotential is typically related to the accumulation of insulating byproducts, which originate from parasitic reactions in the electrolyte or at the carbon electrode.^[19,20,22] However, the ZnO-coated electrode delivered a remarkably enhanced cycle stability over 100 cycles and small charging overpotentials, as observed in Figure 2c,d, which strongly supports the efficacy of ZnO coating on the carbon electrode. Although LiI containing Li-O₂ cell with ZnO-coated cathode showed stable cycle retention, issues related to side reactions involving LiI should be considered including the formation of LiOH due to H-abstraction of solvent molecules or residual water.^[42,43] This phenomenon was known to be severe at high concentration of LiI or water. Nevertheless, in our case, we used 1 M LiTFSI + 0.05 M LiI in TEGDME which contains under 30 ppm H₂O for the cell test, and this low concentration of LiI and H₂O resulted in relatively less side reactions. Also, there were several reports that confirmed enhanced cycle stability using 0.05 M LiI as a redox mediator recently.^[44–46]

To elucidate the enhancement of the Li-O₂ cell performance with the coating, the reactions occurring in each Li-O₂ cell were scrutinized using in situ DEMS during the charge to monitor the evolution of the gas species, as shown in Figure 3. DEMS analyses were also performed with the number of cycles to probe the evolution of the parasitic reactions of the electrolyte and carbon electrode with time/cycling and to determine the extent to which each side reaction was responsible for the

deterioration of the cell. Additional information on the in situ DEMS setup and cell conditions is provided in the Supporting Information. Figure 3 presents the gas analysis results for the first ten cycles of the pristine ¹³C air electrode, where the evolutions of O₂, ¹²CO₂, and ¹³CO₂ gases are shown in red, gray, and blue, respectively, along with the voltage profile in purple. During the first charging process, as shown in Figure 3a, the evolution of oxygen was relatively constant with the typical “M” shape, which is consistent with previous reports.^[22,47–51] The shape of the oxygen evolution curve has been reported to generally hint at the types of the discharge products formed with respect to the crystallinity/stoichiometry or morphology of Li₂O₂.^[22,47–51] Based on the previous studies, we speculate that the oxygen evolution in the first hill of the “M” profile is attributed to the nonstoichiometric Li_{2-x}O₂ film on the electrode, which can be easily decomposed, whereas the oxygen evolution from the second hill originates from the more crystalline or segregated Li₂O₂ (most likely from the solution process), which would involve a slightly higher overpotential during charging.^[52,53] In the Supporting Information, we provide the additional discussions on the origin of the “M” shape, taking account of other possible side reactions such as carbon corrosion and the presence of singlet oxygen.^[19–22,54,55]

The amount of evolved oxygen during first charging was 3.87 μmol, which is far smaller than the theoretically expected value of 9.33 μmol, indicating the occurrence of serious side reactions even in the first cycle, which is common in Li-O₂ batteries.^[56] ¹²CO₂ and ¹³CO₂ started to evolve when the charging voltage was ≈4 V (vs Li/Li⁺), and their evolution gradually increased until the end of charging. Moreover, the Li-O₂ cell with the pristine ¹³C electrode exhibited a significant increase

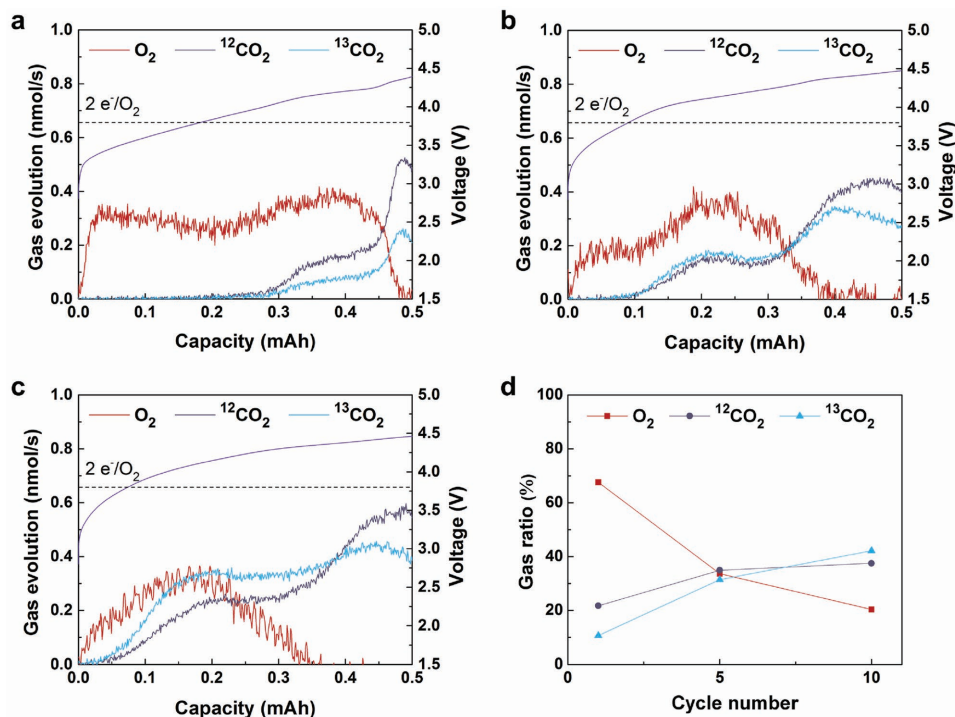


Figure 3. In situ DEMS analyses in Li-O₂ cells with pristine ¹³C cathode during a) first, b) fifth, and c) tenth charge. d) Ratios of evolved gases at pristine ¹³C cathode during cycling.

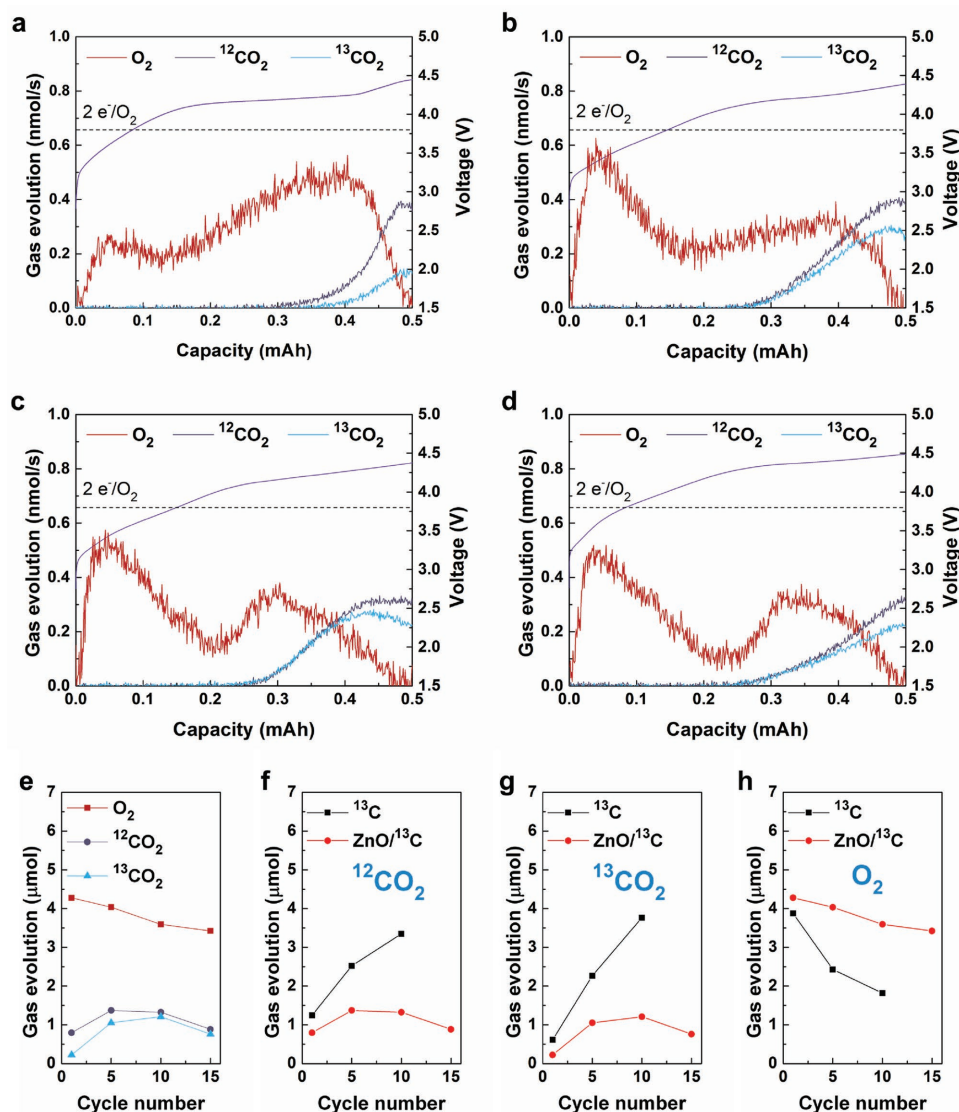


Figure 4. In situ DEMS analyses in Li-O₂ cells with ZnO-coated ¹³C cathode during a) 1st, b) 5th, c) 10th, and d) 15th charge. e) Amounts of evolved gases at the ZnO-coated ¹³C cathode during cycling. Summary of the amounts of f) ¹²CO₂, g) ¹³CO₂, and h) O₂ evolutions during cycling at pristine ¹³C and ZnO-coated ¹³C cathodes.

in the amount of evolved CO₂ gases with the number of cycles, which agrees with previous reports.^[19,22,50] The CO₂ evolution not only indicates the instability of the electrolyte and the carbon cathode but also promotes carbonate formation deteriorating the cell more severely.^[57,58] During the fifth charge, the amount of evolved oxygen was reduced to 2.43 μmol, and the point at which ¹²CO₂ and ¹³CO₂ started to evolve shifted to the beginning of the charging region, resulting in a larger amount of evolved ¹²CO₂ and ¹³CO₂ (Figure 3b). These phenomena became more severe during the tenth charge; the oxygen evolution was reduced to 1.82 μmol, and the “M” shape transformed into a single-hill shape along with the evolution of ¹²CO₂ and ¹³CO₂ upon starting the charging process (Figure 3c). Figure 3d quantitatively compares the relative ratios of the evolved gases with cycling, with the share of oxygen in the entire gas evolution being significantly reduced from 68 to 20% over ten cycles,

accompanied by the rapid cycle degradation of the Li-O₂ cell using the pristine ¹³C air electrode.

The gas analyses for the ZnO-coated electrodes during cycling, however, were quite dissimilar. Figure 4a–d shows the evolution of the gases during the 1st, 5th, 10th, and 15th charge processes from Li-O₂ cells using coated ¹³C air electrodes. Compared with the pristine electrode, the starting point of the CO₂ evolution at charge in Figure 4a is significantly retarded (> 4.2 V vs Li/Li⁺), and the total amounts of CO₂ are also noticeably reduced, whereas the extent of the oxygen evolution is correspondingly higher. More importantly, both ¹²CO₂ and ¹³CO₂ evolution were substantially suppressed, indicating that the ZnO coating subdues the degradation of both the electrolyte and carbon electrode. Considering that the coating could effectively shield the defects in the carbon structure, as illustrated in Figure 1d, this finding support the assumption that the

damaged carbon surface in typical Li-O₂ cells aggravates decomposition of the electrolyte. Notably, the second hill of the oxygen “M” shape increased and the voltage plateau around ≈4.2 V was more pronounced with ZnO coating compared with the pristine ¹³C cathode in Figure 3a. This phenomenon was more dominantly observed with thicker ZnO coating as shown in Figure S7 (Supporting Information) indicating the change in the nature of the Li₂O₂ discharged product with ZnO coating on the carbon air electrode. Compared with the pristine ¹³C electrode for the fifth charge, the coated electrode exhibited more oxygen evolution and greatly reduced amounts of ¹²CO₂ and ¹³CO₂, as observed in Figure 4b, although the CO₂ evolution slightly increased compared with that during the first charge. In addition, the first hill of the “M” shape of the oxygen evolution rose and the second hill was reduced along with shortening of the 4.2 V plateau, whose origin will be discussed later with respect to the stability of ZnO on the carbon surface. In the subsequent 10th and 15th charges in Figure 4c,d, no further significant deterioration of the electrolyte or carbon electrode was observed, and the oxygen evolution profile remained roughly the same. The total amounts of each gas for the ZnO-coated electrode are plotted as a function of cycle number in Figure 4e, revealing no dramatic increase in the CO₂ evolution after five cycles. This finding is in clear contrast to the case of the pristine carbon electrode, as comparatively illustrated in Figure 4f–h for the ¹²CO₂, ¹³CO₂, and O₂ evolutions, respectively, for each air electrode. The total amount of CO₂ evolution in the coated electrode remained approximately the same with a marginal rise or fall, whereas that in the pristine electrode showed rapid growth with cycling, and, in particular, the evolution of ¹³CO₂ gas became more dominant for the later cycles. Interestingly, both the ¹²CO₂ and ¹³CO₂ evolutions showed similar trends of suppression with coating, indicating that the correlated parasitic reactions of the electrolyte and carbon electrode could be inhibited with coating of the electrode. The oxygen evolutions were also maintained with only a slight reduction with cycling, whereas those in the pristine electrode were sharply reduced, as shown in Figure 4h. This finding confirms that the use of a ZnO coating on carbon could successfully enhance the stability of the electrolyte and carbon electrode during the cycling. Nevertheless, the shape of the oxygen evolution profile indicates some changes after cycles, with the first hill becoming slightly larger than the second hill, implying the alteration of the nature of the discharge products with cycles and possible progress of the electrode degradation.

XPS spectra in Figure S9 (Supporting Information) were analyzed to compare chemical states of pristine and ZnO-coated ¹³C electrodes at various cycled states (0, 5, 10, and 15 cycles). As-prepared pristine ¹³C and ZnO-coated ¹³C electrodes showed C–C bondings as a major peak with a signature of C–O bondings along with C–F bondings from the binder (Figure S9a,b, Supporting Information). After five cycles in Figure S9c,d (Supporting Information), C–C bondings decreased and C–O bondings increased with additional formation of O–C=O bondings which stems possibly from carbonate, acetate, or formate. These phenomena were more noticeable for the pristine ¹³C electrode, indicating the suppressed side reactions for the coated carbon electrode in consistent with the DEMS results. After ten cycles in Figure S9e,f (Supporting Information), the

difference between the two electrodes became remarkable. The pristine ¹³C electrode showed an enlarged portion of O–C=O bondings and a negligible signal of C–C bondings, which indicated the excessive accumulation of byproducts by severe side reactions. In contrast, ZnO-coated ¹³C electrode contained only a small portion of O–C=O bondings, although the amount of byproducts increased slightly in comparison with those after five cycles. Besides, C–C bondings remained clear demonstrating that carbon surface was maintained without the significant passivation. After 15 cycles in Figure S9g,h (Supporting Information), O–C=O bondings became larger for both electrodes, while the ZnO-coated ¹³C electrode still displayed the C–C bondings. These XPS data confirmed cleaner carbon surface with ZnO coating, which is well matched with DEMS data that showed subdued side reactions for ZnO-coated carbon electrode.

The stability of the coating was investigated by carefully disassembling the degraded cell and examining the electrode using TEM to understand the gradual change of the gas evolution profile and the possible degradation mechanism. Figure 5a,b presents TEM images of the ZnO-coated electrode after the cell became electrochemically inactive after extended cycling (>100 cycles). Compared with the initial morphology in Figure 1b, most of the ZnO nanoparticles (marked in yellow) were detached from the surface of the carbon after cycling, which is similar to CeO₂ in the previous report.^[59] To confirm this observation and for clearer visualization, we performed similar sets of experiments for the CNT electrode coated with ZnO at different cycle numbers. The TEM images in Figure 5c–f illustrate how the surface-coated ZnO evolves during cycling. After the first discharge in Figure 5c, discharge products were uniformly deposited on both the CNT and ZnO nanoparticles. On the other hand, more Li₂O₂ discharge product began to form at the interface between CNT and ZnO during the third discharge, leading to the detachment of some ZnO nanoparticles from the CNT wall (Figure 5d). However, after the charging process when Li₂O₂ between the carbon surface and ZnO would significantly be reduced in the amount, it appears that ZnO gets stuck to the carbon surface due to the remaining residual Li₂O₂ that may hold the ZnO on the carbon surface to some extent as shown in Figure S8 (Supporting Information). Nevertheless, ZnO already detached after the charge would lose the adhesion to the carbon surface, and more serious detachments were observed after the fifth discharge, as shown in Figure 5e,f. The amount of isolated ZnO nanoparticles continued to increase with increasing cycles. The origin of the Li₂O₂ formation at the interface between carbon and the coating material is not currently clear but we believe that it may depend on several factors such as the binding strength between coating materials and carbon cathode, electrical conductivity of coating material, and the discharge mechanism involving surface coating or precipitation from the solution. Binding strength can be an intuitive and direct index to the detachment. Strong binding between the coating material and carbon would lead to a difficulty for Li₂O₂ to be formed between the two. Also, if the coating material is as electrically conductive as the carbon, Li₂O₂ can be formed relatively easily on the surface of coating materials, which is expected to result in nondetaching coating. On the other hand, if the coating material is insulating, Li₂O₂ cannot

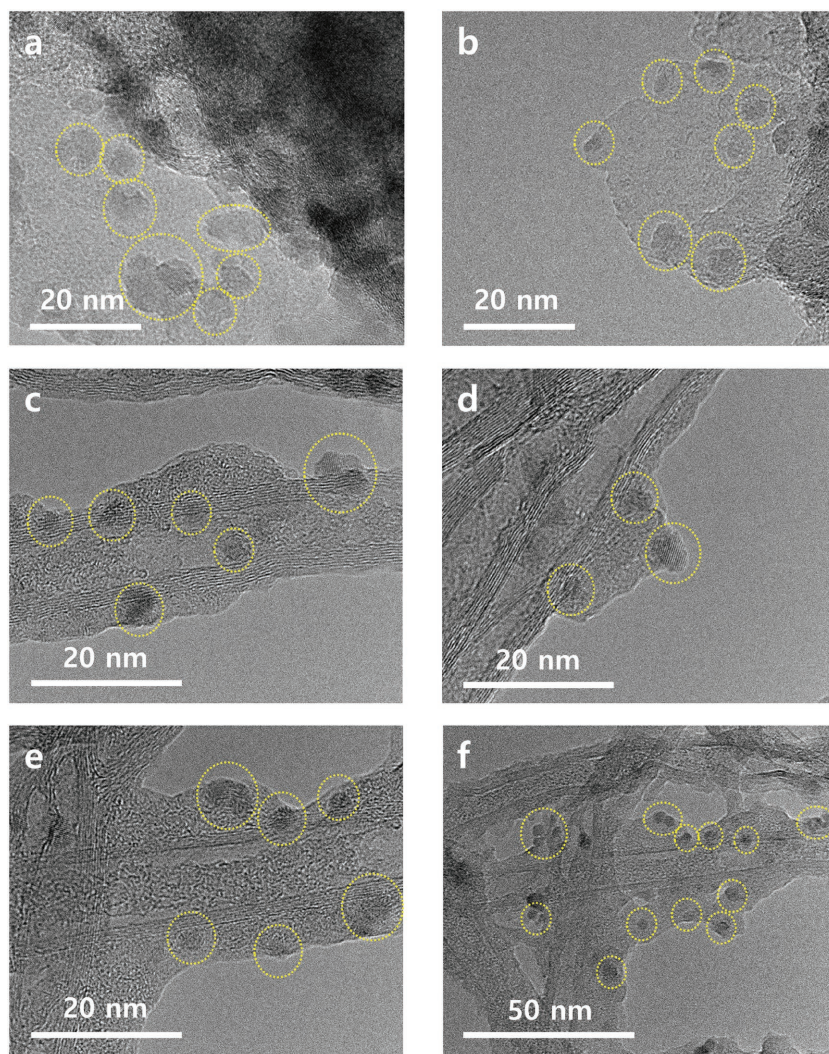


Figure 5. a,b) TEM images of ZnO-coated ^{13}C cathode after cycling. TEM images of ZnO-coated CNT cathode after c) first, d) third, and e,f) fifth discharge.

grow on the surface of coating material, bringing about Li_2O_2 growth primarily between the carbon surface and coating material, and finally fall off of the coating. Based on this speculation, the conductive noble metal oxide or metal particle will suffer less detachment problem. Indeed, previous works showed that FeCo particles were not detached after discharge.^[60] Discharge mechanism can also be closely related to where the discharge product is formed, and coating materials are likely to be less affected by the solution-mediated reaction. The detachment problem implies that the effect of the ZnO coating would be less effective with cycling and may explain the gradual change of the gas evolution behavior and the capacity degradation with extended cycles.

3. Conclusion

The effect of surface coating on a carbon air electrode was investigated using isotope ^{13}C carbon and in situ DEMS analysis.

The ZnO-coated carbon air electrode was highly resistant to side reactions both in the electrolyte and carbon air electrode, which resulted in enhanced cycle performance. In contrast to the pristine carbon electrode, the coating provided effective protection, which reduced the evolution of undesirable gases from both the electrolyte ($^{12}\text{CO}_2$) and carbon electrode ($^{13}\text{CO}_2$), with high efficiency of O_2 evolution. Nevertheless, the coating materials were gradually detached from the surface of the carbon materials because of the formation of a discharge product at the interface between the carbon and coating materials during cycling, leading to exposure of the bare carbon electrode and degradation of the Li-O_2 cell. This study suggests that a method to prevent the detachment of the coating material as well as further understanding of the growth mechanism of discharge products, which affects the delamination of the coating, should be sought after in the future.

4. Experimental Section

Preparation of Air Electrodes: The active carbon materials composed of ^{13}C (97%) were purchased from Cambridge Isotope Laboratory. The conventional air electrode for the Li-O_2 cell was fabricated using a mixture of the prepared ^{13}C carbon and binder (Kynar 2801) with a weight ratio of 90:10. The mixture was dispersed in N-methyl-2-pyrrolidone (NMP, Sigma-Aldrich, 99.5%) and cast onto a Ni-mesh current collector (1/2 in. diameter). The loading densities of the ^{13}C electrodes were $\approx 1 \text{ mg cm}^{-2}$. The freestanding CNT air electrodes used as a reference were synthesized using the following procedure. First, 40 mg of the CNTs (CM 250, Hanwa Chemical, Korea) was dispersed in 80 mL of deionized (DI) water containing a small amount of poly(4-styrenesulfonic acid) (PSS, $M_w = 75\,000$, 18 wt% in H_2O , Sigma-Aldrich, USA) and mixed in a sonicator for 1 h. A stable CNT dispersion with a concentration of 0.5 mg mL^{-1} was obtained. The mixture was then sonicated for 10 min and filtered using a polyvinylidene fluoride (PVDF) filter membrane (pore size: $0.45 \mu\text{m}$, diameter: 47 mm, Millipore, USA). The filtered films were dried in ambient air for 12 h before being peeled off from the membrane. The CNT papers were then cut into 3/8 in. diameter fragments for use as freestanding electrodes. The loading densities of the freestanding CNT electrodes were $\approx 0.25 \text{ mg cm}^{-2}$. ALD of ZnO and Al_2O_3 on the carbon electrodes was performed in a laminar flow ALD reactor (CN-1 Co., Ltd., ATOMIC-CLASSIC 2nd edition) consisting of a chamber, canisters, mass flow controllers, pneumatic valves, a pressure gage, and a pump. The carbon electrodes were loaded on the center of the reactor for 30 min at 150°C in high-purity N_2 ($>99.999\%$) flow to reach thermal equilibrium and outgas the carbon electrodes. To measure the thickness of the ZnO and Al_2O_3 coatings on the electrode, a bare Si wafer was loaded concurrently as a reference in the same chamber, and its thickness was measured using a spectroscopic ellipsometer (SE, MG-1000, NanoView). Diethyl zinc (DEZ, Nuritech Co., Ltd.) was employed as the zinc precursor, and water was used as the oxygen precursor to deposit ZnO. For the Al_2O_3 coating, trimethylaluminum

(TMA, Nuritech Co.) and water were used as the aluminum and oxygen precursors, respectively. The supplements of each precursor were $\approx 1.3 \times 10^{-4}$, 4.5×10^{-5} , and 1.3×10^{-3} mol s^{-1} for DEZ, TMA, and water, respectively. All the precursors were vaporized from external canisters at room temperature and led into the chamber. The deposition processes of ZnO and Al₂O₃ consisted of four steps: metal precursor (DEZ or TMA) dosing (0.5 s)–N₂ purge (10 s)–H₂O dosing (1 s)–N₂ purge (10 s). For purging the reactor, N₂ gas was used at a flow rate of 400 sccm. All the delivery lines were maintained at 100 °C. The base pressure of the reactor was less than 10 mTorr, and ALD was performed at a working pressure of 0.2–1.7 Torr. ZnO was deposited on the carbon electrode for 8, 15, and 50 cycles, which correspond to 0.5, 2.5, and 10 nm thicknesses of the ZnO film on the Si wafer. These samples were denoted as 8-cyc, 15-cyc, and 50-cyc ZnO/carbon. Ten cycles of Al₂O₃ correspond to an Al₂O₃ film thickness of 0.5 nm on the Si wafer and it was denoted as 10-cyc Al₂O₃.

Preparation of Protected Li Metal: The composite protective layer (CPL) on Li metal was fabricated using a simple doctor-blading and roll-pressing method. The CPL slurry was prepared by mixing 0.8 g of 480 nm sized Al₂O₃ (AES-II, Ishihara Inc., Japan) and 0.2 g of PVDF-HFP in 0.6 g of propylene carbonate (PC) ($\geq 99.7\%$, Sigma-Aldrich, USA) and 0.9 g of dimethylacetamide (DMAc) ($\geq 99.9\%$, Sigma-Aldrich, USA) for 24 h. The CPL was coated on a glass plate using a doctor blade (blade thickness = 150 μ m; Honzo, Japan) and then dried at room temperature for 1 h in vacuum to evaporate the DMAc. The freestanding CPL was spontaneously detached from the glass substrate, and the PC in the CPL was removed in a DI water bath. Then, the CPL was dried at 60 °C for 2 d in vacuum to completely remove any residual water and subsequently stored in an Ar-filled glove box. The CPL was laminated on a Li metal foil (450 μ m) by roll-pressing at room temperature.

Preparation of Li-O₂ Cells: Li metal foil (7/16 in. diameter) or CPL-coated Li metal, a glass fiber separator (Whatman GF/F microfiber filter paper, 0.7 μ m pore size), the electrolyte, and the prepared air electrodes were stacked in sequence in a Swagelok-type cell. The electrolyte was 1 M LiTFSI in TEGDME, and 0.05 M LiI was added into the electrolyte for the redox mediator test. The electrolyte contain <30 ppm water (determined by Karl Fischer titration). All the cells were assembled in a glove box (H₂O < 0.5 ppm, O₂ < 0.5 ppm) and operated in an O₂ atmosphere (770 Torr). Each cell was relaxed for 1 h in an O₂ atmosphere and operated using the capacity-limited mode of 0.5 mA h (¹³C electrode) and 1000 mA h g⁻¹ (CNT electrode) within the voltage range of 2.0–4.5 V. All the cells were galvanostatically discharged and charged at a current density of 0.1 mA cm⁻². A potentiogalvanostat (WBCS 3000, WonA Tech, Korea) was used to measure the electrochemical properties.

Characterization: The morphologies of the samples were examined using scanning electron microscopy (SEM, MERLIN Compact, ZEISS, Germany) and TEM (JEM2100F, JEOL, Japan). The chemical compositions of the air electrodes were probed using XPS (Thermo VG Scientific). The Raman spectra (LabRam HR, Horiba Jobin-Yvon, France) were recorded using a continuous-wave linearly polarized laser (wavelength: 514.5 nm; 2.41 eV; power: 16 mW). In situ gas detection spectrometry was carried out to analyze the gases evolving from the Li-O₂ cell, by purging the cell with an Ar carrier gas (10 mL min⁻¹) continuously during charging. Simultaneously, the Ar carrier gas with gaseous products was pumped off to $\approx 10^{-7}$ Torr with rotary pump and turbomolecular pump sequentially (differential pumping), and then transferred to quadrupole mass spectrometer (MS; HPR-20, Hiden Analytical, UK). Before the DEMS experiment, the cells were initially discharged and then connected to the MS being fully relaxed in the Ar flow for 4 h before charging. During charging, electrochemical reaction and concomitant gas evolution from the cell were analyzed concurrently. The MS was calibrated for O₂, CO₂, and Ar with the use of known gas concentrations (2000 ppm O₂, 2000 ppm CO₂/Ar balance) to establish linear relationship between the gas concentration and ion current.

Supporting Information

Supporting Information is available from the Wiley Online Library or from the author.

Acknowledgements

This work was supported by the Samsung Advanced Institute of Technology and a National Research Foundation of Korea (NRF) grant funded by the Korea government (MSIP) (No. 2015R1A2A1A10055991). Y.-S.M. was partially supported by the Korea Institute of Energy Technology Evaluation and Planning (KETEP: 20153030013060) and the Korea Evaluation Institute of Industrial Technology (KEIT: 10063277).

Conflict of Interest

The authors declare no conflict of interest.

Keywords

atomic layer deposition, carbon defect, in situ differential electrochemical mass spectroscopy, lithium–oxygen batteries, stability

Received: September 22, 2017

Revised: November 22, 2017

Published online: February 14, 2018

- [1] M. Armand, J.-M. Tarascon, *Nature* **2008**, 451, 652.
- [2] R. Black, B. Adams, L. Nazar, *Adv. Energy Mater.* **2012**, 2, 801.
- [3] P. G. Bruce, S. A. Freunberger, L. J. Hardwick, J.-M. Tarascon, *Nat. Mater.* **2012**, 11, 19.
- [4] G. Girishkumar, B. McCloskey, A. Luntz, S. Swanson, W. Wilcke, *J. Phys. Chem. Lett.* **2010**, 1, 2193.
- [5] M. S. Whittingham, *Chem. Rev.* **2004**, 104, 4271.
- [6] M. D. Bhatt, H. Geaney, M. Nolan, C. O'Dwyer, *Phys. Chem. Chem. Phys.* **2014**, 16, 12093.
- [7] Y.-C. Lu, Y. Shao-Horn, *J. Phys. Chem. Lett.* **2012**, 4, 93.
- [8] H. Kim, H.-D. Lim, J. Kim, K. Kang, *J. Mater. Chem. A* **2014**, 2, 33.
- [9] S. J. Kang, T. Mori, S. Narizuka, W. Wilcke, H.-C. Kim, *Nat. Commun.* **2014**, 5, 3937.
- [10] Y. Bae, H.-D. Lim, Y. S. Yun, K. Kang, *J. Electrochem. Sci. Technol.* **2014**, 5, 49.
- [11] H. D. Lim, K. Y. Park, H. Song, E. Y. Jang, H. Gwon, J. Kim, Y. H. Kim, M. D. Lima, R. O. Robles, X. Lepró, R. H. Baughman, K. Kang, *Adv. Mater.* **2013**, 25, 1348.
- [12] H. D. Lim, H. Song, J. Kim, H. Gwon, Y. Bae, K. Y. Park, J. Hong, H. Kim, T. Kim, Y. H. Kim, X. Lepró, R. Ovalle-Robles, R. H. Baughman, K. Kang, *Angew. Chem., Int. Ed.* **2014**, 53, 3926.
- [13] H.-D. Lim, H. Song, H. Gwon, K.-Y. Park, J. Kim, Y. Bae, H. Kim, S.-K. Jung, T. Kim, Y. H. Kim, X. Lepró, R. Ovalle-Robles, R. H. Baughman, K. Kang, *Energy Environ. Sci.* **2013**, 6, 3570.
- [14] Z. K. Luo, C. S. Liang, F. Wang, Y. H. Xu, J. Chen, D. Liu, H. Y. Sun, H. Yang, X. P. Fan, *Adv. Funct. Mater.* **2014**, 24, 2101.
- [15] R. Mi, H. Liu, H. Wang, K.-W. Wong, J. Mei, Y. Chen, W.-M. Lau, H. Yan, *Carbon* **2014**, 67, 744.
- [16] W.-H. Ryu, T.-H. Yoon, S. H. Song, S. Jeon, Y.-J. Park, I.-D. Kim, *Nano Lett.* **2013**, 13, 4190.
- [17] G. Wu, N. H. Mack, W. Gao, S. Ma, R. Zhong, J. Han, J. K. Baldwin, P. Zelenay, *ACS Nano* **2012**, 6, 9764.

- [18] J. Xie, X. Yao, Q. Cheng, I. P. Madden, P. Dornath, C. C. Chang, W. Fan, D. Wang, *Angew. Chem.* **2015**, 127, 4373.
- [19] M. M. O. Thotiyl, S. A. Freunberger, Z. Peng, P. G. Bruce, *J. Am. Chem. Soc.* **2012**, 135, 494.
- [20] B. McCloskey, A. Speidel, R. Scheffler, D. Miller, V. Viswanathan, J. Hummelshøj, J. Nørskov, A. Luntz, *J. Phys. Chem. Lett.* **2012**, 3, 997.
- [21] D. M. Itkis, D. A. Semenenko, E. Y. Kataev, A. I. Belova, V. S. Neudachina, A. P. Sirotnina, M. Hävecker, D. Teschner, A. Knop-Gericke, P. Dudin, *Nano Lett.* **2013**, 13, 4697.
- [22] Y. Bae, Y. S. Yun, H.-D. Lim, H. Lee, Y.-J. Kim, J. Kim, H. Park, Y. Ko, S. Lee, H. J. Kwon, H. Kim, H.-T. Kim, D. Im, K. Kang, *Chem. Mater.* **2016**, 28, 8160.
- [23] M. Leskes, A. J. Moore, G. R. Goward, C. P. Grey, *J. Phys. Chem. C* **2013**, 117, 26929.
- [24] B. M. Gallant, R. R. Mitchell, D. G. Kwabi, J. Zhou, L. Zuin, C. V. Thompson, Y. Shao-Horn, *J. Phys. Chem. C* **2012**, 116, 20800.
- [25] S. A. Freunberger, Y. Chen, N. E. Drewett, L. J. Hardwick, F. Bardé, P. G. Bruce, *Angew. Chem., Int. Ed.* **2011**, 50, 8609.
- [26] Z. Peng, S. A. Freunberger, Y. Chen, P. G. Bruce, *Science* **2012**, 337, 563.
- [27] M. M. O. Thotiyl, S. A. Freunberger, Z. Peng, Y. Chen, Z. Liu, P. G. Bruce, *Nat. Mater.* **2013**, 12, 1050.
- [28] W.-J. Kwak, H.-G. Jung, S.-H. Lee, J.-B. Park, D. Aurbach, Y.-K. Sun, *J. Power Sources* **2016**, 311, 49.
- [29] X. Gao, Y. Chen, L. R. Johnson, Z. P. Jovanov, P. G. Bruce, *Nat. Energy* **2017**, 2, 17118.
- [30] J.-J. Xu, X.-B. Zhang, *Nat. Energy* **2017**, 2, 17133.
- [31] J. Lu, Y. Lei, K. C. Lau, X. Luo, P. Du, J. Wen, R. S. Assary, U. Das, D. J. Miller, J. W. Elam, H. M. Albishri, D. A. El-Hady, Y.-K. Sun, L. A. Curtiss, K. Amine, *Nat. Commun.* **2013**, 4, 2383.
- [32] J. Elam, D. Routkevitch, S. George, *J. Electrochem. Soc.* **2003**, 150, G339.
- [33] Y.-S. Min, I. H. Lee, Y. H. Lee, C. S. Hwang, *CrystEngComm* **2011**, 13, 3451.
- [34] Y.-S. Min, E. J. Bae, J. B. Park, U. J. Kim, W. Park, J. Song, C. S. Hwang, N. Park, *Appl. Phys. Lett.* **2007**, 90, 263104.
- [35] E. Yilmaz, C. Yogi, K. Yamanaka, T. Ohta, H. R. Byon, *Nano Lett.* **2013**, 13, 4679.
- [36] F. Li, Y. Chen, D.-M. Tang, Z. Jian, C. Liu, D. Golberg, A. Yamada, H. Zhou, *Energy Environ. Sci.* **2014**, 7, 1648.
- [37] Q.-C. Liu, J.-J. Xu, Z.-W. Chang, X.-B. Zhang, *J. Mater. Chem. A* **2014**, 2, 6081.
- [38] J. Schwan, S. Ulrich, V. Batori, H. Ehrhardt, S. Silva, *J. Appl. Phys.* **1996**, 80, 440.
- [39] B. J. Bergner, A. Schürmann, K. Peppler, A. Garsuch, J. Janek, *J. Am. Chem. Soc.* **2014**, 136, 15054.
- [40] W.-J. Kwak, D. Hirshberg, D. Sharon, M. Afri, A. A. Frimer, H.-G. Jung, D. Aurbach, Y.-K. Sun, *Energy Environ. Sci.* **2016**, 9, 2334.
- [41] D. J. Lee, H. Lee, Y. J. Kim, J. K. Park, H. T. Kim, *Adv. Mater.* **2016**, 28, 857.
- [42] W.-J. Kwak, D. Hirshberg, D. Sharon, H.-J. Shin, M. Afri, J.-B. Park, A. Garsuch, F. F. Chesneau, A. A. Frimer, D. Aurbach, Y.-K. Sun, *J. Mater. Chem. A* **2015**, 3, 8855.
- [43] C. M. Burke, R. Black, I. R. Kochetkov, V. Giordani, D. Addison, L. F. Nazar, B. D. McCloskey, *ACS Energy Lett.* **2016**, 1, 747.
- [44] S. H. Yoon, Y. J. Park, *Sci. Rep.* **2017**, 7, 42617.
- [45] J. Kang, J. Kim, S. Lee, S. Wi, C. Kim, S. Hyun, S. Nam, Y. Park, B. Park, *Adv. Energy Mater.* **2017**, 7, 1700814.
- [46] B. G. Kim, C. Jo, J. Shin, Y. Mun, J. Lee, J. W. Choi, *ACS Nano* **2017**, 11, 1736.
- [47] D. Kundu, R. Black, E. J. Berg, L. F. Nazar, *Energy Environ. Sci.* **2015**, 8, 1292.
- [48] D. Oh, K. Virwani, L. Tadesse, M. Jurich, N. Aetukuri, L. E. Thompson, H.-C. Kim, D. S. Bethune, *J. Phys. Chem. C* **2017**, 121, 1404.
- [49] S. M. Ahn, J. Suk, D. Y. Kim, Y. Kang, H. K. Kim, D. W. Kim, *Adv. Sci.* **2017**, 4, 1700235.
- [50] D. W. Kim, S. M. Ahn, J. Kang, J. Suk, H. K. Kim, Y. Kang, *J. Mater. Chem. A* **2016**, 4, 6332.
- [51] Y. Chang, S. Dong, Y. Ju, D. Xiao, X. Zhou, L. Zhang, X. Chen, C. Shang, L. Gu, Z. Peng, G. Cui, *Adv. Sci.* **2015**, 2, 1500092.
- [52] B. D. Adams, C. Radtke, R. Black, M. L. Trudeau, K. Zaghib, L. F. Nazar, *Energy Environ. Sci.* **2013**, 6, 1772.
- [53] Y. Zhang, Q. Cui, X. Zhang, W. C. McKee, Y. Xu, S. Ling, H. Li, G. Zhong, Y. Yang, Z. Peng, *Angew. Chem., Int. Ed.* **2016**, 55, 10717.
- [54] J. Wandt, P. Jakes, J. Granwehr, H. A. Gasteiger, R.-A. Eichel, *Angew. Chem.* **2016**, 128, 7006.
- [55] N. Mahne, B. Schafzahl, C. Leypold, M. Leypold, S. Grumm, A. Leitgeb, G. A. Strohmeier, M. Wilkening, O. Fontaine, D. Kramer, C. Slugovc, S. M. Borisov, S. A. Freunberger, *Nat. Energy* **2017**, 2, 17036.
- [56] B. D. Adams, R. Black, C. Radtke, Z. Williams, B. L. Mehdi, N. D. Browning, L. F. Nazar, *ACS Nano* **2014**, 8, 12483.
- [57] S. R. Gowda, A. Brunet, G. M. Wallraff, B. D. McCloskey, *J. Phys. Chem. Lett.* **2013**, 4, 276.
- [58] S. Zhang, M. J. Nava, G. K. Chow, N. Lopez, G. Wu, D. R. Britt, D. G. Nocera, C. C. Cummins, *Chem. Sci.* **2017**, 8, 6117.
- [59] C. Yang, R. A. Wong, M. Hong, K. Yamanaka, T. Ohta, H. R. Byon, *Nano Lett.* **2016**, 16, 2969.
- [60] W.-J. Kwak, T.-G. Kang, Y.-K. Sun, Y. J. Lee, *J. Mater. Chem. A* **2016**, 4, 7020.